





Article

On the Effect of the M^{3+} Origin on the Properties and Aldol Condensation Performance of MgM^{3+} Hydrotalcites and Mixed Oxides

Valeriia Korolova ¹, Oleg Kikhtyanin ², Martin Veselý ³, Dan Vrtiška ¹, Iva Paterová ³, Vlastimil Fíla ⁴, Libor Čapek ⁵ and David Kubička ^{1,2,*}

- ¹ Department of Petroleum Technology and Alternative Fuels, University of Chemistry and Technology Prague, Technická 5, 166 28 Prague, Czech Republic; korolovv@vscht.cz (V.K.); vrtiskad@vscht.cz (D.V.)
- ² Technopark Kralupy, University of Chemistry and Technology Prague, nám. G. Karse 7/2, 278 01 Kralupy nad Vltavou, Czech Republic; oleg.kikhtyanin@vscht.cz
- ³ Department of Organic Technology, University of Chemistry and Technology Prague, Technická 5, 166 28 Prague, Czech Republic; veselyr@vscht.cz (M.V.); dudkovai@vscht.cz (I.P.)
- ⁴ Department of Inorganic Technology, University of Chemistry and Technology Prague, Technická 5, 166 28 Prague, Czech Republic; filav@vscht.cz
- ⁵ Department of Physical Chemistry, Faculty of Chemical Technology, University of Pardubice, Studentská 573, 532 10 Pardubice, Czech Republic; libor.capek@upce.cz
- * Correspondence: kubickad@vscht.cz



Citation: Korolova, V.; Kikhtyanin, O.; Veselý, M.; Vrtiška, D.; Paterová, I.; Fíla, V.; Čapek, L.; Kubička, D. On the Effect of the M^{3+} Origin on the Properties and Aldol Condensation Performance of MgM^{3+} Hydrotalcites and Mixed Oxides. *Catalysts* **2021**, *11*, 992. <https://doi.org/10.3390/catal11080992>

Academic Editors: Ioan-Cezar Marcu and Octavian Dumitru Pavel

Received: 2 August 2021

Accepted: 17 August 2021

Published: 18 August 2021

Publisher's Note: MDPI stays neutral with regard to jurisdictional claims in published maps and institutional affiliations.



Copyright: © 2021 by the authors. Licensee MDPI, Basel, Switzerland. This article is an open access article distributed under the terms and conditions of the Creative Commons Attribution (CC BY) license (<https://creativecommons.org/licenses/by/4.0/>).

Abstract: Hydrotalcites (HTCs) are promising solid base catalysts to produce advanced biofuels by aldol condensation. Their main potential lies in the tunability of their acid-base properties by varying their composition. However, the relationship between the composition of hydrotalcites, their basicity, and their catalytic performance has not yet been fully revealed. Here, we investigate systematically the preparation of HTCs with the general formula of $Mg_6M^{3+}_2(OH)_{16}CO_3 \cdot 4H_2O$, where M^{3+} stands for Al, Ga, Fe, and In, while keeping the Mg/M^{3+} equal to 3. We use an array of analytical methods including XRD, N_2 physisorption, CO_2 -TPD, TGA-MS, FTIR-ATR, and SEM to assess changes in the properties and concluded that the nature of M^{3+} affected the HTC crystallinity. We show that the basicity of the HTC-derived mixed oxides decreased with the increase in atomic weight of M^{3+} , which was reflected by decreased furfural conversion in its aldol condensation with acetone. We demonstrate that all MgM^{3+} mixed oxides can be fully rehydrated, which boosted their activity in aldol condensation. Taking all characterization results together, we conclude that the catalytic performance of the rehydrated HTCs is determined by the “host” MgO component, rather than the nature of M^{3+} .

Keywords: hydrotalcites; mixed oxides; aldol condensation; basic catalysts

1. Introduction

The Green Chemistry principles aroused a strong interest in the development of solid base catalysts for important base-catalyzed reaction, such as transesterification, aldol condensation, or alkylation [1–9]. The use of solid base catalysts would allow for reducing the amount of produced waste waters significantly along with simplifying the product separation and improving the product quality. Magnesium-containing mixed oxides are among the most studied materials as they can be prepared rather easily by calcination of the so-called hydrotalcites (HTCs), i.e., hydroxycarbonates with layered structure and the general formula $[M^{2+}_{1-x}M^{3+}_x(OH)_2]^{b+}[A^{n-}]_{b/n} \cdot mH_2O$, where M^{2+} and M^{3+} are divalent and trivalent metal cations, respectively, and A is an interlayer anion, typically carbonate [1,10,11]. Besides Mg, Zn or Ni are used as divalent cations, whereas the trivalent cations are represented primarily by Al that can be replaced e.g., by Ga or Fe [1,9,12–17]. Due to the so-called memory effect, the mixed oxides having a Lewis-base character can

be rehydrated to form hydrotalcites in hydroxide form (instead of the carbonate form) with a Brønsted-base character [2,3,18]. This opens not only a range of the application possibilities, but also of the fundamental questions relating to the relationship between their structure and basicity as well as between their physico-chemical properties and catalytic performance.

The acid–base properties of HTC-based catalysts for organic reactions can be tailored by isomorphous substitution of Mg and Al cations with various other di- and trivalent cations [12,13,19]. The basicity of M^{2+} Al hydrotalcites decreased when Mg was replaced by Zn or Ni which was reflected in the catalytic performance of the HTC-derived materials [19–22]. However, the effect of Al substitution by another M^{3+} element in the MgM^{3+} hydrotalcite-like materials on their acid-base properties and catalytic performance has not yet been systematically described.

Aldol condensation is currently used to synthesize fine chemicals [5,23,24], and it holds a promising potential for development of sustainable aviation fuels [25–28] and bio-based monomers [29,30]. In addition, it is a suitable reaction for probing the acid-base character of catalysts as only the accessible, i.e., catalytically active basic sites can be reached by the reactants in both mixed oxides and reconstructed hydrotalcites. In contrast, the common CO_2 -TPD method is suitable for probing the basic sites only in mixed oxides as the rehydrated hydrotalcites react with CO_2 and are transformed into hydroxycarbonates [16]. Moreover, CO_2 can also reach those basic sites that are not accessible to the reactants, i.e., sites relevant to CO_2 adsorption and storage, but not to catalysis.

The wide variability of the typically used hydrotalcite synthesis protocols including their activation by calcination yielding mixed oxides and by calcination followed by rehydration affording reconstructed hydrotalcites and their use in different reactions under varying reaction conditions thwart the fundamental evaluation of the specific influence of the M^{3+} cation on the structure and activity of the synthesized materials. Therefore, we have synthesized a series of MgM^{3+} hydrotalcites with M^{3+} being Al, Ga, Fe, and In using the same synthesis procedure and evaluated the derived mixed oxides and reconstructed hydrotalcites with respect to their physico-chemical properties and catalytic performance in aldol condensation of furfural and acetone. This allowed us to elucidate the role of the trivalent cation on the structure, properties, and catalytic performance (including its stability) of the synthesized materials.

2. Results and Discussion

2.1. Catalyst Synthesis and Characterization

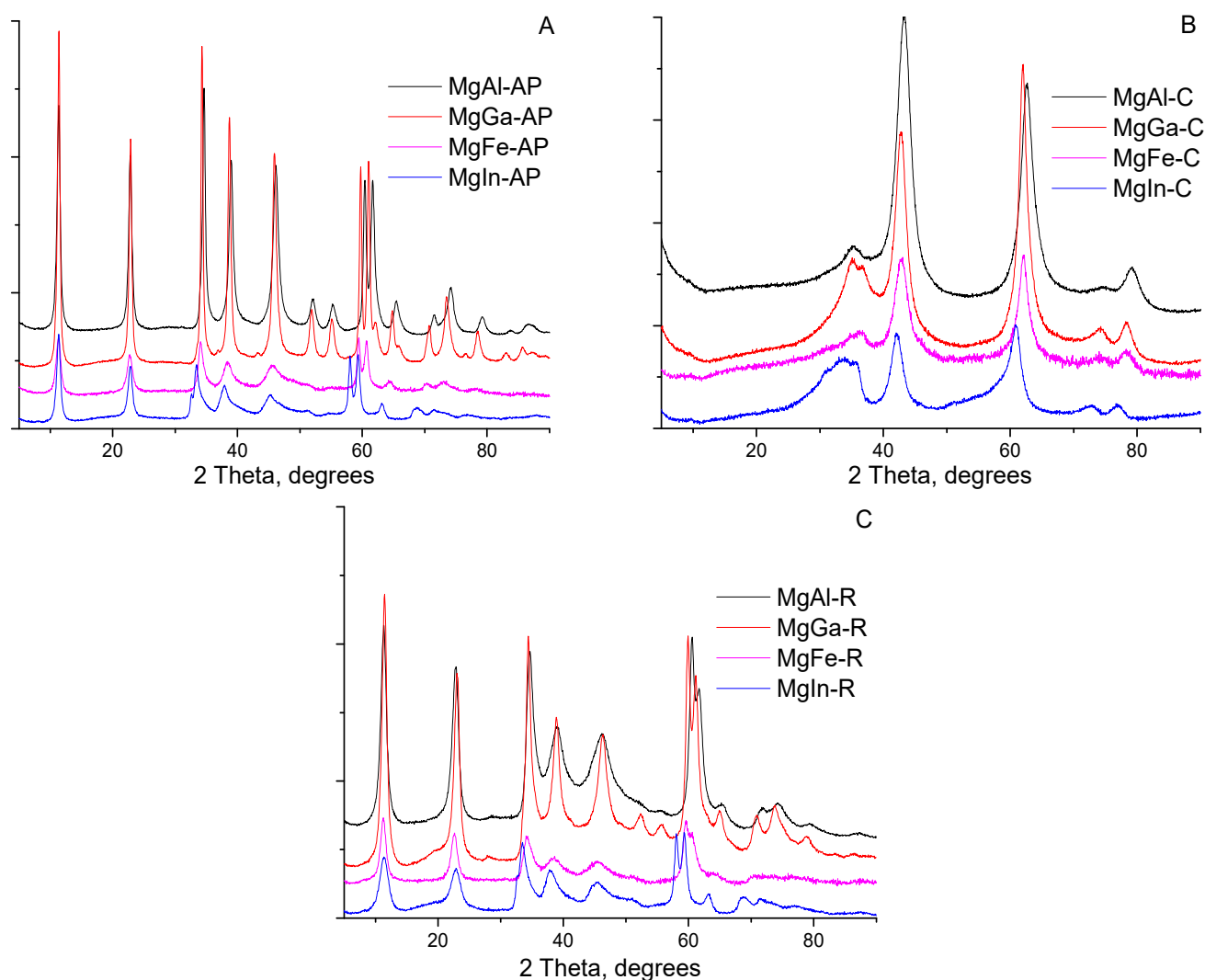
The ICP and XRD results confirmed that the coprecipitation of magnesium nitrate and the corresponding M^{3+} nitrate (M^{3+} being Al, Ga, In, and Fe, respectively) by the alkaline solution of Na_2CO_3 and NaOH resulted in the formation of the respective hydrotalcite with the targeted Mg/M^{3+} ratio of 3. The ICP results also proved that sodium that could interfere in the catalytic studies was removed almost completely during washing of the precipitates. The Na/M^{3+} atomic ratio was in the range 0.025–0.033 and did not reveal any dependence on the M^{3+} nature.

The measured Mg/M^{3+} atomic ratios are reported in Table 1 together with the calculated formula of the as prepared hydrotalcites. The calculation was possible as phase pure hydrotalcite phases characterized by the diffraction lines at $2\theta \approx 11.3^\circ, 22.5^\circ, 34.5^\circ, 39^\circ, 46^\circ, 60^\circ,$ and 61.5° were formed (Figure 1A) without any admixtures being detectable. The formation of the phase-pure HTC materials suggested an effective substitution of Mg^{2+} cations in the brucite-like layers by M^{3+} cations (even in case of In^{3+} with the largest ionic radius of 0.8 Å) being in line with the previous studies [16,17,31,32].

Table 1. Mg/M³⁺ atomic ratios in the as-prepared samples according to ICP results and the proposed HTC formula.

Sample	Ionic Radius of M ³⁺ , Å *	Mg ²⁺ /M ³⁺ by ICP	Proposed Chemical Formula of Prepared Solids	Theoretical Weight Loss under Calcination
MgAl-AP	0.535	3.0	Mg ₆ Al ₂ (OH) ₁₆ CO ₃ ·4H ₂ O	43.1
MgGa-AP	0.62	2.8	Mg _{5.6} Ga ₂ (OH) _{15.2} CO ₃ ·3.8H ₂ O	34.6
MgFe-AP	0.645	2.9	Mg _{5.8} Fe ₂ (OH) _{15.6} CO ₃ ·3.9H ₂ O	38.0
MgIn-AP	0.8	2.9	Mg _{5.8} In ₂ (OH) _{15.6} CO ₃ ·3.9H ₂ O	32.2

*—from <http://abulafia.mt.ic.ac.uk/shannon/ptable.php> (Accessed on 2 July 2021).

**Figure 1.** XRD patterns of as-prepared (A), calcined (B), and rehydrated (C) MgAl, MgGa, MgFe, and MgIn samples.

Although all as-prepared samples exhibited the hydrotalcite structure, the intensity of the reflections in the XRD patterns differed significantly (Figure 1) indicating difference in crystallinity. The crystallinity was evaluated using the area of the signals attributed to two different basal reflections (003 and 110) and is reported as relative crystallinity (Table 2). MgGa-AP and MgAl-AP were the most crystalline among the samples with the crystallinity close to 100%, followed by MgFe-AP and MgIn-AP with the crystallinity of 32–41% (Figure 1A and Table 2). Such a difference in the crystallinity could either reflect the impact of M³⁺ cations on the dimensions of HTC platelets and the existence of local defects in the layered structure or suggest the presence of X-ray amorphous impurities.

Table 2. Crystallinity, lattice parameters, and crystallite size (L(Å)) of the prepared samples.

Sample	Relative Crystallinity (%)	HTC Basal Spacing d_{003} , (Å)	Unit Cell a , (Å)	MgO		Crystallite Size, L (Å)		
				d_{200} , (Å)	d_{003}	d_{110}	d_{200}	d_{220}
MgAl-AP	98	7.8	3.063		116	188		
MgGa-AP *	100	7.81	3.096		153	231		
MgFe-AP	32	7.85	3.111		86	143		
MgIn-AP	41	7.83	3.178		98	157		
MgAl-C				2.089			30	31
MgGa-C				2.107			40	46
MgFe-C				2.119			33	40
MgIn-C				2.141			39	45
MgAl-R	88	7.83	3.061		57	85		
MgGa-R	95	7.78	3.088		78	127		
MgFe-R	29	7.85	3.103		62	78		
MgIn-R	38	7.81	3.172		54	114		

*—the sample with the largest crystallinity taken as a reference.

The diffraction lines assigned to (003) and (110) reflections (i.e., at $\approx 11.3^\circ$ and 60°) were used to calculate the basal spacing between the layers (d_{003}) and the unit cell dimension a (as $a = 2d_{110}$), respectively. The d_{003} value increased from 7.80–7.81 Å to 7.83–7.85 Å with the increase in the ionic radius of M^{3+} cations (Table 2), which reflected the change in the thickness of each hydroxide layer due to the change in the charge density of the layers [33]. The unit cell dimension increased linearly from 3.063 Å to 3.178 Å with the increase in the M^{3+} ionic radius (Table 2). Both diffraction lines were used to calculate the sizes of the crystallites in the direction of the layers stacking (d_{003}) and of the layers plane (d_{110}). The dimensions are given in Table 2; they correlate well with the relative crystallinity values, i.e., the larger the crystallinity, the larger the crystallite size (i.e., the size of the coherent domain).

The hydrotalcite structure of all samples was completely decomposed because of the calcination at 450 °C and the corresponding mixed oxide phase was formed as evidenced by the diffraction lines at $2\theta \approx 43.0^\circ$ and 62.5° (Figure 1B). These reflections are characteristic for the periclase structure (MgO). Nonetheless, the presence of M^{3+} cations in the MgO structure can be deduced from the increase in the MgO basal spacing in the calcined samples, d_{200} , from 2.089 Å to 2.141 Å with the increasing ionic radius of M^{3+} . It is noteworthy that the average crystallite size (L) of the MgM-C samples calculated from d_{200} and d_{220} basal reflections was considerably lower than the crystallite size of the corresponding as-prepared hydrotalcites (Table 2). Unfortunately, the presence of other plausible phases, in particular spinel and isolated M^{3+} oxides, can be neither excluded nor confirmed by the XRD data.

It is well documented that the HTC-derived mixed oxides, when rehydrated, can be reconstructed to the original hydrotalcite structure. This has been demonstrated mainly for MgAl materials [18,34–39], but some examples of successful transformation of MgGa, MgFe, and MgIn mixed oxides to hydrotalcites exist as well [16,17,31,40]. It worth noting that rehydrated MgIn HTC was previously obtained only by the hydrothermal treatment of a corresponding MgIn mixed oxide (140 °C, 24 h) in Na_2CO_3 solution [31]. By using the same rehydration procedure, we have succeeded in transforming all MgM^{3+} mixed oxides to the corresponding hydrotalcites as evidenced by the appearance of the characteristic HTC diffraction lines at $2\theta \approx 11.3, 22.5, 34.5^\circ$, etc. and disappearance of the mixed oxide diffraction lines at $2\theta \approx 43.0^\circ$ and 62.5° (Figure 1C). In particular, the reconstruction of the MgIn HTC structure by the treatment of MgIn mixed oxide with pure water at ambient temperature has not yet been reported. A comparison of the diffractograms in Figure 1A,C shows that the intensities of the XRD reflexes of the rehydrated samples are much smaller than those of the as prepared hydrotalcites. However, as demonstrated in Table 2, the relative crystallinity of the rehydrated samples was not significantly lower than that of the as-prepared hydrotalcites.

The unit cell size (Table 2) of the rehydrated materials was only slightly lower than in case of the as prepared HTC, but it preserved its linear dependence on the M^{3+} ionic radius. While the crystallinity and unit cell size were preserved, there was a dramatic decrease in the size of the coherent domains in both directions, i.e., in the stacking (d_{003}) as well as in the platelet plane (d_{110}) (Table 2). The results indicate that, although the crystalline structure was reconstructed and the unit cell size was virtually unchanged due to rehydration, there were some imperfections due to the rehydration process that resulted in the observed decrease in the crystallite size, i.e., in the coherent domain size. This can be plausibly explained by the incomplete insertion of the M^{3+} cations in their original positions in the brucite-like layers (which is supported by the observed decrease in the unit cell size) and the formation MgM^{3+} spinel or M^{3+} oxide phases that break the structure periodicity and thus reduce the coherent domain size. Apparently, the extent is rather small as neither of these phases was detected by XRD, i.e., their coherent domain sizes were too small.

The visual inspection of prepared materials using SEM revealed differences in the morphology of the samples due to the differences in the M^{3+} element and due to the calcination-rehydration treatments (Figure 2). Regardless of the M^{3+} cation in the structure, all AP-HTCs showed a well-developed layered structure with haphazardly oriented and intergrown platelets (Figure 2). These agglomerates were several micrometers large and consisted of differently sized platelets (<1 mm). While MgAl-AP and MgGa-AP had well-shaped platelets (0.3–0.6 and 0.5–0.8 mm, respectively, (Figure 2), the platelets of MgFe-AP and MgIn-AP were more heterogeneous and layered character was less developed, particularly in case of MgIn-AP. These observations are in line with the relative crystallinity data based on XRD (Table 2), i.e., the samples with higher crystallinity have larger and well-organized platelets.

Upon calcination and calcination followed by rehydration, the size of the agglomerates did not change significantly, but the shape and degree of heterogeneity increased because of the rehydration treatment. This is demonstrated on the MgGa-R, i.e., the sample with the highest crystallinity among rehydrated samples, in Figure 2 (2R) (enlarged image is available in Figure S1 in the SI). In great contrast to MgGa-AP, the MgGa-R platelets were crumbled, and their surface was cracked which supports the observed decrease in the coherent domain size (Table 2). A similar trend was observed for all the MgM^{3+} rehydrated materials. Consequently, the individual platelets of MgIn-R could be barely distinguished (Figure 2).

The textural properties of the AP hydrotalcites reflected the relative crystallinity of the samples, i.e., the BET surface area decreased linearly with the increasing relative crystallinity of the AP-HTCs (Tables 2 and 3), and it also decreased with the increasing crystallite size (d_{003} and d_{110}) determined from the XRD data (Table 2). A similar trend was also observed for the total pore volume. The calcination affording mixed oxides resulted in a tremendous increase in the BET area (2 to 7 times) and total pore volume (1.5 to 3 times) in comparison with the AP-HTCs (Table 3). Again, the BET surface decreases linearly with the increasing crystallite size of the mixed oxides (d_{200} and d_{220}), proving that the crystallite size (the coherent domain size) is the decisive structural parameter affecting the specific surface area of both AP-HTCs and mixed oxides.

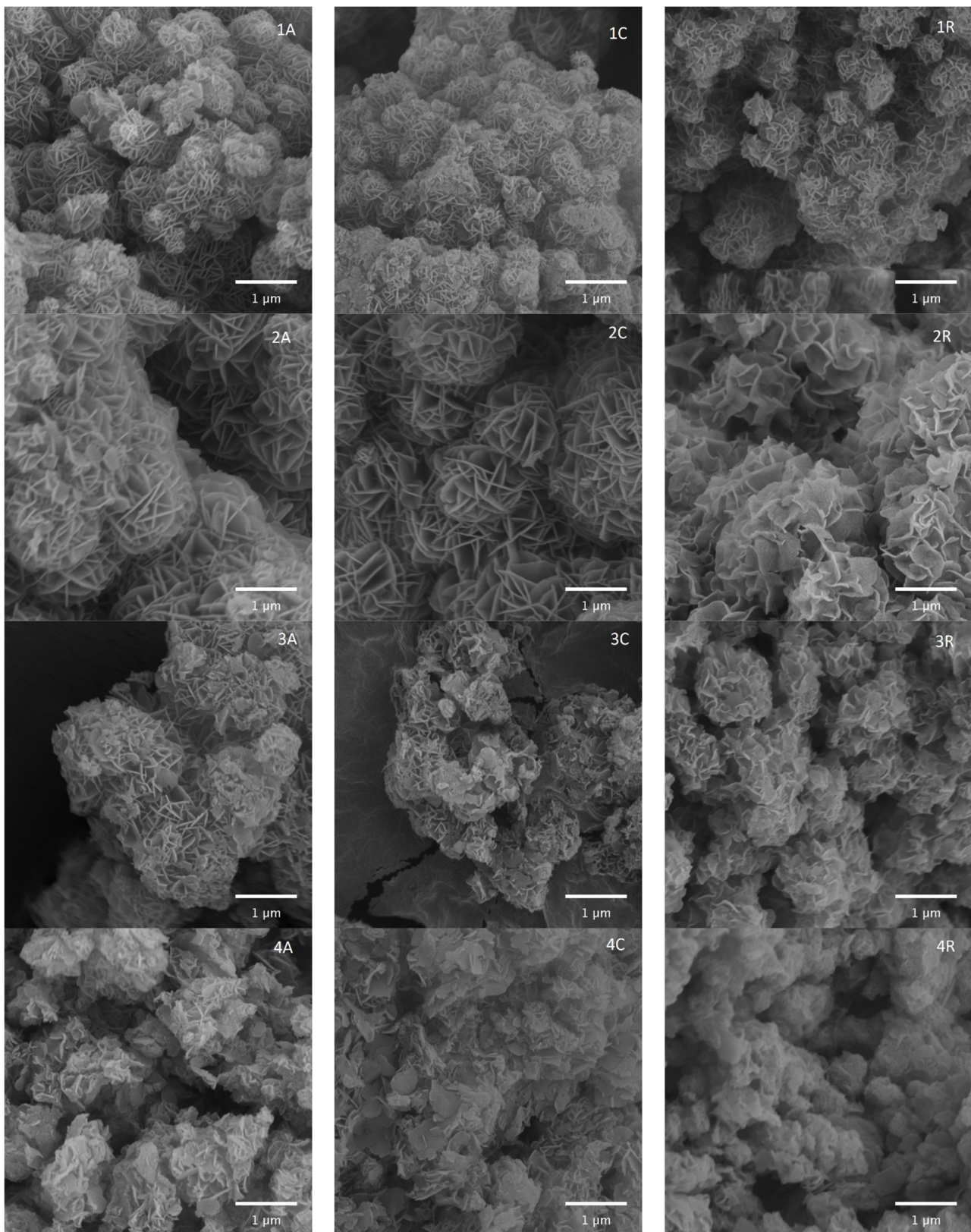


Figure 2. Scanning electron micrographs of the prepared samples: 1—MgAl, 2—MgGa, 3—MgFe, 4—MgIn. A—as-prepared, C—calcined, R—rehydrated for 20 min.

Table 3. BET surface of the as-prepared hydrotalcites (AP), derived mixed oxides (C), and rehydrated hydrotalcites (R), as well as the basic properties of MgM-C samples.

Material	BET Surface Area (m ² /g)			Pore Volume (cm ³ /g)			Concentration of Basic Sites in MgM-C, $\mu\text{mol/g}$	Density of Basic Sites in MgM-C, $\mu\text{mol/m}^2$	Calculated Ratio $\mu\text{mol}_{\text{CO}_2}/\mu\text{mol}_{\text{Mg}^{2+}}$ in MgM-C
	AP	C	R	AP	C	R			
MgAl	31	222	5	0.094	0.343	0.013	270	1.2	0.015
MgGa	34	164	4	0.095	0.221	0.011	225	1.4	0.017
MgFe	103	185	12	0.275	0.416	0.031	171	0.9	0.012
MgIn	76	134	19	0.196	0.288	0.039	167	1.3	0.015

On the other hand, the calcination followed by rehydration resulted in very low BET surface areas ($<20 \text{ m}^2/\text{g}$, i.e., only 12–25% of the BET value obtained for the AP-HTCs) of the MgM-R materials that is in contrast with the decreased crystallite size of the rehydrated HTCs in comparison with their AP counterparts. Thus, there has to be an additional parameter affecting the textural properties. The most plausible explanation is the presence of anions and water molecules in the interlayer space blocking access or the existence of local defects. This conclusion is supported by the trend among the MgM-R materials where the materials with larger platelets (as seen on SEM images, Figure 2) have smaller BET area and total pore volume (Table 3).

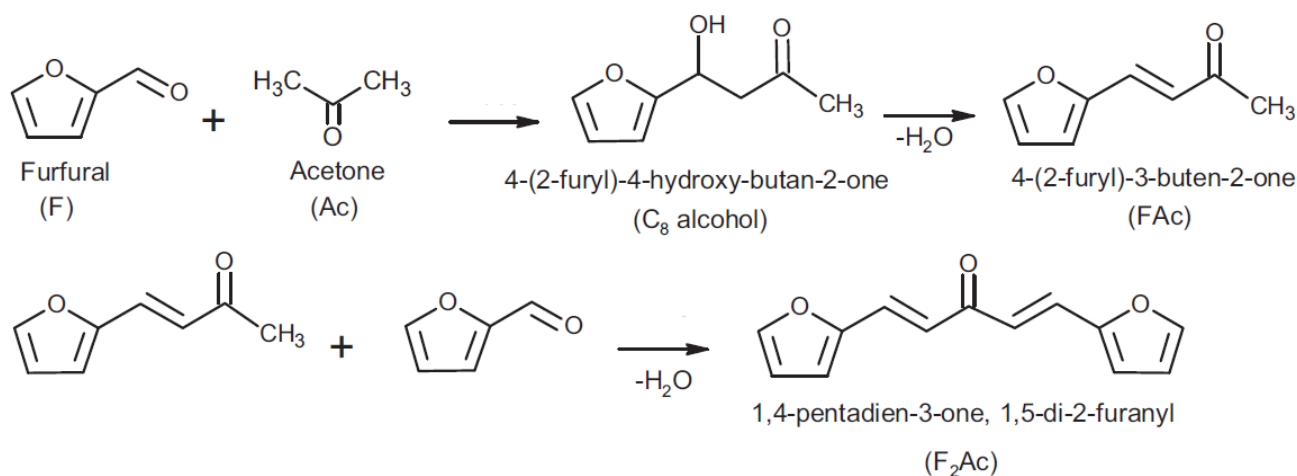
The structural changes due to calcination leading to MgM mixed oxides and due to calcination and rehydration affording MgM rehydrated hydrotalcites were further corroborated by the FTIR (Figure S2) and TGA-MS (Figure S3) characterization results that are presented in detail in the SI. The total weight loss observed in the TGA-MS experiments decreased logically with the increasing atomic weight of the M^{3+} cation (Figure S3), and it agreed with the theoretical weight loss calculated from the MgM-AP HTC composition (Table 1). It can be thus inferred that the AP hydrotalcites are indeed phase pure HTCs having the composition reported in Table 1. Moreover, the ratio of the weight loss of a MgM-R to the weight loss of the corresponding MgM-AP was close to unity (Figure S3), which provides more evidence that nearly complete reconstruction of the HTC structure by mixed oxide rehydration was achieved independently on the nature of the M^{3+} cation.

The structural changes in the MgM materials due to differences in composition as well as calcination and rehydration treatments also affect the number and character of the acid and base sites that are essential for the catalytic activity of these materials. The number of basic sites in MgM-C was determined using CO_2 -TPD (Figure S4 in the SI) and the results are reported in Table 3. There is a clear increase in the number of basic sites with the decrease in ionic radius of the M^{3+} cation. Nonetheless, it has to be noted that the number of basic sites is given per one gram of the material, i.e., when keeping the atomic ratio of Mg/M^{3+} constant, the relative content of Mg in one gram of sample increases with the decreasing atomic weight of M^{3+} . As a result, the specific Mg content correlates with the number of basic sites. Thus, when normalizing the number of basic sites per 1 mol of Mg^{2+} rather than 1 g of mixed oxide, a constant value of 0.015 mmol of basic sites (adsorbed CO_2) per 1 mmol of Mg atoms is obtained (Table 3). In other words, the number of basic sites is a function of the Mg content per 1 g of material and, thus, the M^{3+} cation does not contribute to the basic character and a simple “spacer” between the Mg-related basic sites can be seen. In addition, the CO_2 desorption profiles were virtually identical for all MgM-C materials which indicated that the strength of CO_2 adsorption, i.e., the strength of the basic sites, was not influenced by the M^{3+} cation nature (Figure S3 in the SI).

2.2. Catalyst Performance

The changes in the catalyst properties resulting from the replacement of Al^{3+} by other M^{3+} elements as well as due to the calcination and rehydration treatments were further characterized by their performance in aldol condensation of furfural with acetone. The basic scheme of aldol condensation of furfural with acetone is shown in Scheme 1.

In general, furfural (F) reacts with acetone (Ac) forming a hydrated intermediate, 4-(2-furyl)-4-hydroxybutan-2-one (FAC-OH) that dehydrates giving a first condensation product, 4-(2-furyl)-3-buten-2-one (FAC). The FAC can react with another F resulting in the formation of 1,4-pentadien-3-one, 1,5-di-2-furanyl (F_2Ac) as the second condensation product. The plausible self-condensation of acetone over mixed oxides was insignificant corresponding to acetone conversion <2% and thus did not affect the aldol condensation of F with Ac. Moreover, the catalyst leaching was also excluded following an approach described previously [41]. The total carbon mass balance including the reactants and the major reaction products, i.e., FAC-OH, FAC, and F_2Ac always exceeded 95%. Heavier reaction products, most likely due to consecutive condensation reactions, were observed only at high furfural conversion. Due to their poor identification and low concentration, they were excluded from the carbon balance calculation.



Scheme 1. Basic reaction scheme of aldol condensation between furfural with acetone (from [34]).

In preliminary experiments, the catalytic performance of the four as-prepared materials was evaluated in aldol condensation of furfural and acetone at $T = 50\text{ }^\circ\text{C}$ and acetone:furfural ratio of 10. Independently from the origin of M^{3+} , furfural conversion was below 1.5% in all cases, thus proving the absence of a strong basicity in the as-prepared HTCs.

The furfural conversion and selectivity to all three main products at $50\text{ }^\circ\text{C}$ over MgM-C mixed oxides are summarized in Figures 3A and 3B, respectively. The initial reaction rate decreased in order $\text{MgAl-C} > \text{MgGa-C} > \text{MgIn-C} > \text{MgFe-C}$ (Figure 3A). After the initial rapid increase in F conversion (ca. the initial 40 min), the F conversion continued to grow only moderately, which can be ascribed to the gradual catalyst reaction either due to the deposition of heavier products formed by consecutive condensation reactions or due to the specific blockage of basic sites, e.g., by furoic acid formed by Cannizzaro reaction [42]. The initial reaction rate (reflecting the rate of furfural disappearance during initial 10 min, $\text{mmol}_F \cdot \text{g}_{\text{cat}}^{-1} \cdot \text{min}^{-1}$) increased linearly with an increase in the number of basic sites per gram in a catalyst demonstrating the role of basic sites (Figure 4A). From the catalyst synthesis point of view, it follows that smaller M^{3+} cations are preferred as they allow for increasing the number of basic sites per gram of catalysts while maintaining the same Mg/M^{3+} ratio. The reaction rate data also exhibit positive correlation with the BET surface area of the calcined samples, thus indicating the importance of the accessibility of the active sites (Figure 4B). These two positive correlations at the same time suggest that the surface density of the basic sites ($\mu\text{mol}/\text{m}^2$) does not affect to a great extent in the studied range ($0.9\text{--}1.4\ \mu\text{mol}/\text{m}^2$, Table 3) the reaction rate.

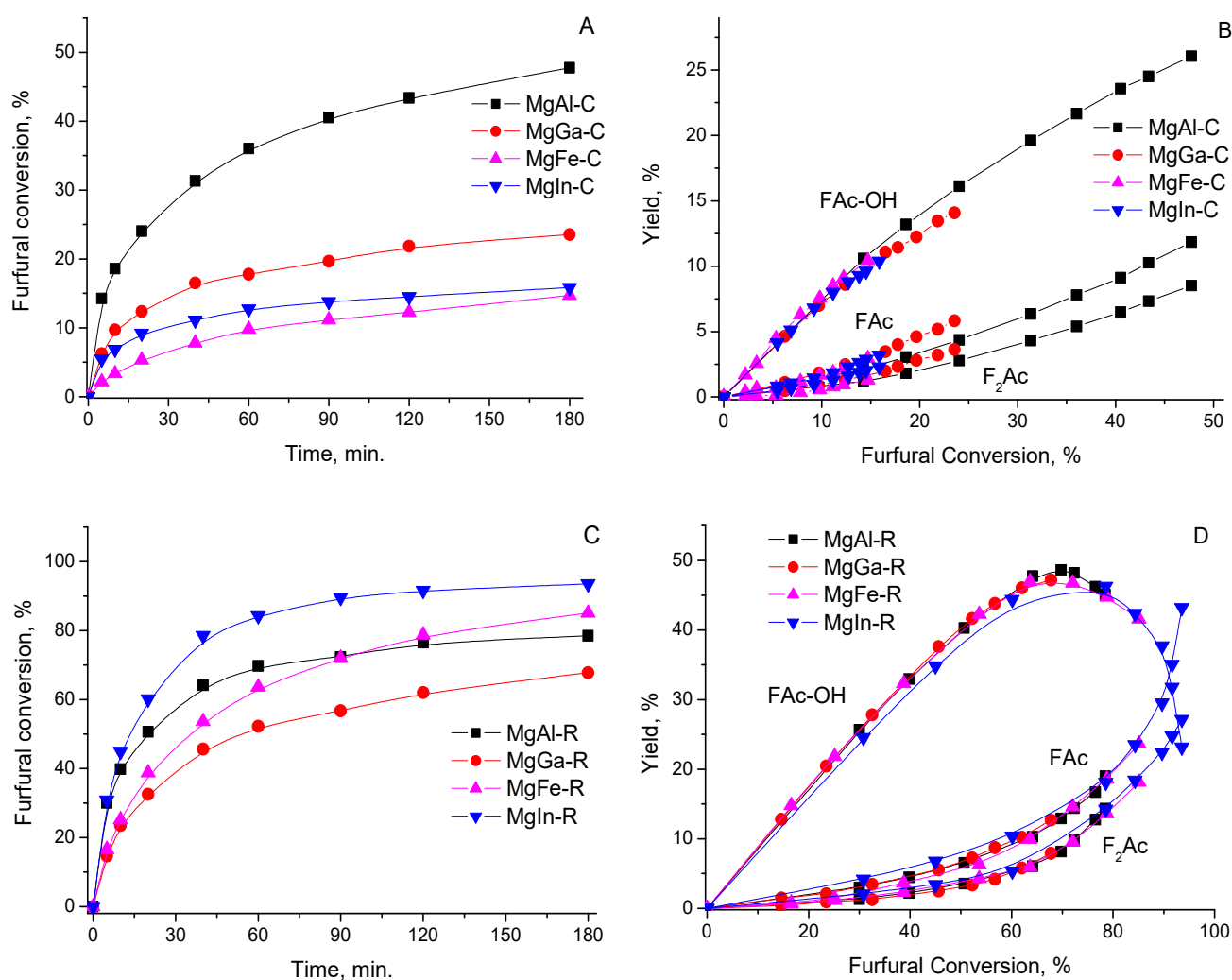


Figure 3. The dependence of the furfural conversion on the reaction time observed on MgM-C ((A), $T_{\text{reac.}} = 50\text{ }^{\circ}\text{C}$, molar ratio F:Ac = 1:10) and MgM-R (C), $T_{\text{reac.}} = 25\text{ }^{\circ}\text{C}$, molar ratio F:Ac = 1:5) samples. Yield for the reaction products is observed on MgM-C (B) and MgM-R (D) as a function of the furfural conversion.

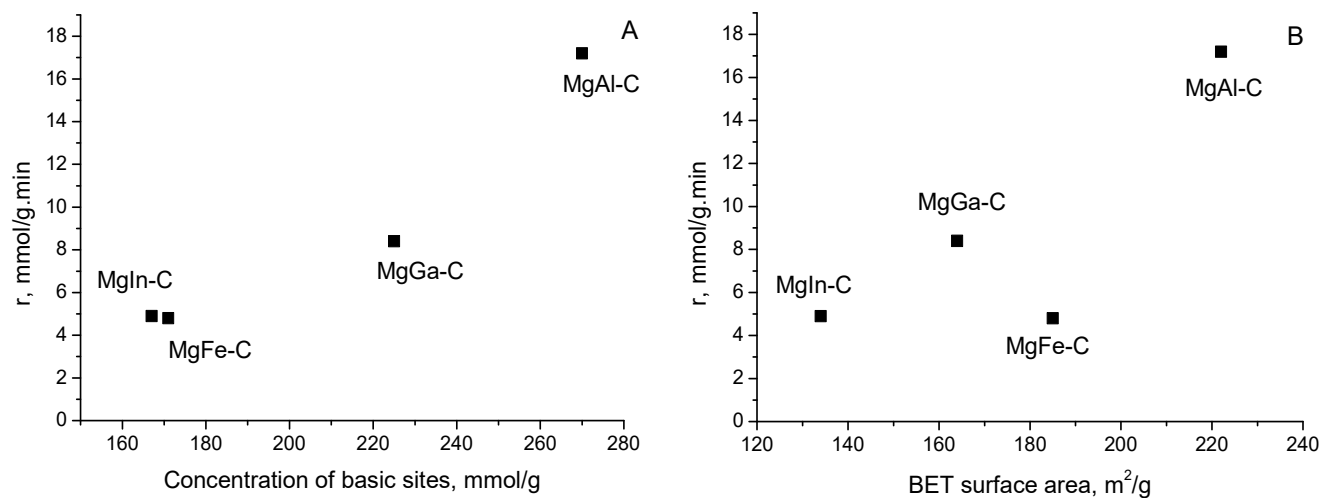


Figure 4. The dependence of the initial reaction rate on the concentration of basic sites (A) and BET surface area (B) of MgM-C samples.

The selectivity to the main products was virtually identical at a given conversion regardless of the nature of the M^{3+} and the number and concentration of basic sites (Figure 3B). It can be, thus, inferred that all MgM^{3+} mixed oxides possessed the same nature of basic sites, i.e., that MgO provided the basic sites, with a similar strength as seen by TPD results (Figure S4 in the SI). In conclusion, the M^{3+} cation determines the number of available basic sites (per gram of catalyst) in MgM^{3+} mixed oxides, but it does not affect either the type or the strength of the basic sites present. Moreover, the linear relationship between the initial activity and the number of basic sites also indicates that either all basic sites determined by CO_2 desorption or their same percentage in all MgM^{3+} mixed oxides are accessible to the reactants and take part in the reaction.

The rehydration of the MgM^{3+} mixed oxides has resulted in a significant increase in the aldol condensation rate as documented in Figure 3C. Despite the aldol condensation reaction using rehydrated HTCs being performed at only 25 °C, significantly higher F conversion was obtained than over the MgM^{3+} mixed oxide catalysts at 50 °C (Figure 3A). While for MgAl materials successful rehydration resulting in the transformation of the Lewis basic sites into the more intrinsically active Bronsted basic sites is well known [2,34,43,44], it has been reported only scarcely for MgGa and MgFe materials [16,17,40]. A successful rehydration of MgIn mixed oxide is reported for the first time and the rehydrated MgIn-R HTC was even found to be a more efficient catalyst for aldol condensation of F and Ac. In line with the aldol condensation over mixed oxides reported here and the previous studies on aldol condensation, the superior performance of the MgIn-R catalyst should be related to its superior number of accessible basic sites.

Due to the chemical reaction between rehydrated hydrotalcites, i.e., materials in exclusively hydroxy form, with CO_2 resulting in the replacement of some hydroxyls and formation of the more stable and thermodynamically-favored hydroxycarbonates, TPD- CO_2 cannot be used to determine the number of basic sites. Nonetheless, the catalytic data can be used to compare the number of basic sites in different rehydrated catalysts. The data in Figure 3C show that the initial reaction rate decreased in the order $MgIn \approx MgAl > MgFe \approx MgGa$. As with the MgM^{3+} mixed oxides, the decrease in catalytic activity was observed at longer reaction times (>40 min) and the final conversion decreased in the order $MgIn > MgFe > MgAl > MgGa$ (Figure 3C), which can be concluded to be also the order of the number of accessible basic sites. As in the case of $MgM-C$ catalysts, all $MgM-R$ have also exhibited a virtually identical selectivity to the main reaction products (Figure 3D). It suggests that the upon-rehydration created Bronsted basic sites had similar strength distribution, i.e., the differences in the observed conversion have to be caused by other catalyst properties than by their base-sites strength.

The inspection of the specific BET surface areas of the rehydrated $MgM-R$ materials further supports the significantly higher intrinsic catalytic activity of the Bronsted basic sites than of the Lewis basic sites as the BET area of the rehydrated materials was 7 to 26 times lower (Table 3) than that of their mixed oxide counterparts. Interestingly, the most severe drop (20- to 26-times lower BET for $MgM-R$ than for $MgM-C$) was observed for MgAl and MgGa, i.e., the most crystalline materials. In contrast, the BET decrease only 7- to 13-times for the less crystalline MgFe and MgIn rehydrated catalysts (Table 3). These results agree with the observed decrease in catalyst activity at longer reaction times (Figure 3C) as the rehydrated HTC catalysts with the largest BET surface area (MgIn-R and MgFe-R) exhibited a weaker decrease in the catalyst activity (i.e., a larger difference between the final conversion and the conversion after ca. 10 min) than MgAl-R and MgGa-R that had a similar initial activity as MgIn-R and MgFe-R, respectively (Figure 3C). As discussed above, the textural data (BET area, total pore volume) are further corroborated by the relative crystallinity results (XRD) and by the HTC platelets size (SEM). In particular, the decreasing size of the rehydrated HTC platelets corresponds well to the increasing furfural conversion (Figure 5). This is in line with the findings of Abello et al. [2] who suggested that only the active sites located at the edges of the platelets were operative in aldol condensations. As the formation of smaller platelets inherently increases the number of OH^- ions near

the edges, the reconstructed HTC with a smaller size of HTC platelets should possess enhanced catalytic activity.

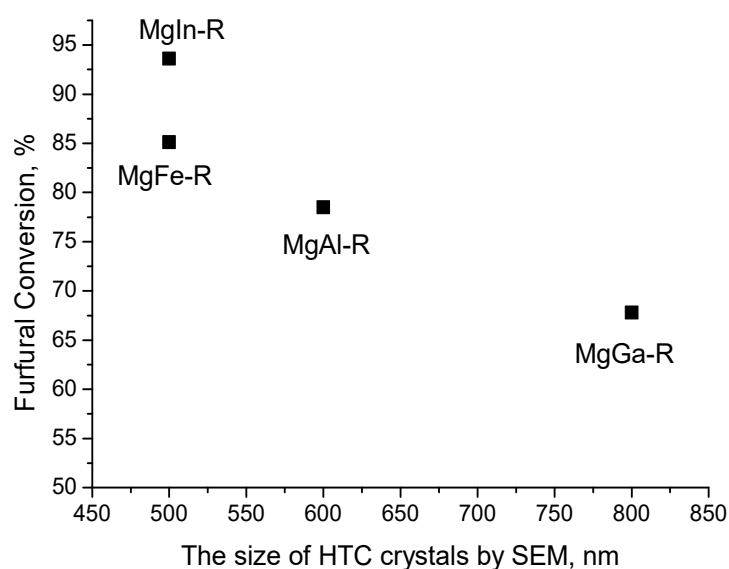


Figure 5. A correlation between the size of HTC platelets in rehydrated MgM-R20 hydroxalclites evaluated by SEM and furfural conversion over these catalysts after 180 min of the reaction.

The stability of the MgM^{3+} catalysts was assessed in the consecutive catalytic cycles consisting always of calcination, rehydration, and reaction (Figure 6A). All studied MgM-R catalysts exhibited stable catalytic performance without any obvious significant change in furfural conversion during the three catalytic cycles (Figure 6A). In fact, in the consecutive experiments with MgAl-R and MgGa-R, an increase in the conversion of furfural was observed in comparison with the first experiment, while MgFe-R and MgIn-R maintained its conversion in the second and third run on the same level (Figure 6A). The catalyst stability was further supported by the stable yields of all three main reaction products as a function of furfural conversion independently on the nature of the M^{3+} cation and regardless of the number of consecutive runs (Figure 6B). Once again, this shows the indirect catalytic role of the M^{3+} cation, i.e., it was not involved directly in the aldol condensation reaction.

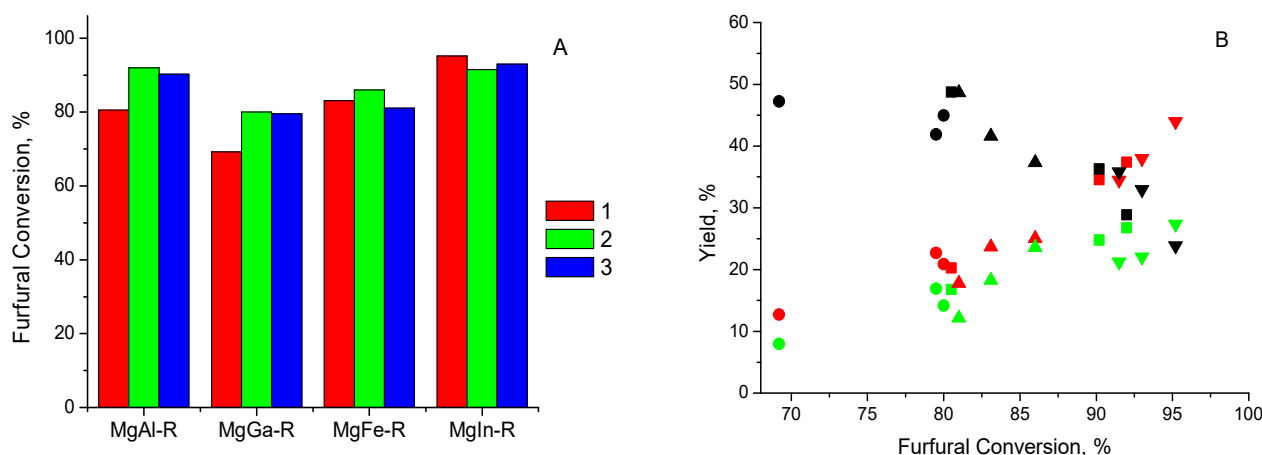


Figure 6. (A). Furfural conversion in three consecutive cycles [calcination-rehydration-reaction] in the presence of different MgM-R materials; (B) the yield of reaction products observed in three reaction cycles. Black symbols—FAC-OH, red symbols—FAC, green symbols—F₂Ac; squares—MgAl-R, circles—MgGa-R, triangle up—MgFe-R, triangle down—MgIn-R. Molar ratio furfural: acetone = 5, $T_{\text{reac.}}$ = 25 °C, reaction time—3 h.

3. Experimental Materials and Methods

3.1. Catalyst Preparation

MgM³⁺ hydrotalcite (HTC) samples (where M stands for Al, Ga, Fe, and In) with a Mg/M³⁺ atomic ratio in a reactive mixture of 3:1 were prepared based on a coprecipitation method adopted from [34,41]. Mg(NO₃)₂·6H₂O (99.9%, Lach:NER, Neratovice, Czech Republic), Al(NO₃)₃·9H₂O (98.8%, Lach:NER, Czech Republic), Ga(NO₃)₃·xH₂O (99.9%, Sigma-Aldrich, Prague, Czech Republic), Fe(NO₃)₃·9H₂O (98%, Sigma-Aldrich) and In(NO₃)₃·xH₂O (99.9%, Sigma-Aldrich) were used to prepare a salt solution, while NaOH (99.6%, Lach:NER, Czech Republic) and Na₂CO₃ (99%, Penta, Czech Republic) were used to prepare an alkaline solution. An aqueous solution of Mg and M³⁺ nitrates (total metal ion concentration of 0.5 mol·L⁻¹) was slowly added to 200 mL of redistilled water. The flow rate of the simultaneously added alkaline solution of Na₂CO₃ (0.2 mol·L⁻¹) and NaOH (1 mol·L⁻¹) was controlled to maintain the reaction pH at the desired value (10.0 ± 0.1). The coprecipitation was carried out for 3 h under vigorous stirring (450 rpm) at 25 °C. The resulting suspension was then aged at 25 °C under stirring for 1.5 h. The precipitate was then filtered, washed several times with a plenty of distilled water (at least 2 L), and dried for 12 h at room temperature and then for 12 h at 60 °C. Finally, the as-prepared MgM³⁺ HTCs (further denoted as MgM-AP) were calcined in static air at 450 °C for 3 h in a muffle oven to produce the corresponding MgM mixed oxides (further denoted as MgM-C) and transferred into a desiccator at the end of the calcination procedure to avoid contamination by atmospheric CO₂ during cooling. The rehydration of the mixed oxides was performed by their stirring at 200 RPM in water (0.5 g of freshly calcined material per 100 mL of redistilled water) at room temperature for 20 min, followed by filtration of the resulting solid (further denoted as MgM-R) using a Buchner funnel equipped with a vacuum pump. The MgM-R samples were immediately transferred into a reactor loaded with furfural and acetone to initiate aldol condensation.

3.2. Physico-Chemical Characterization

The phase composition of the prepared catalysts was determined by X-ray diffraction using a diffractometer PANanalytical X'Pert3 Powder and CuK α radiation. The XRD patterns were recorded in a range of 2 θ = 5–70°. The relative crystallinity (%) of the as-prepared MgM HTCs and rehydrated HTCs was estimated from the area of signals at the diffraction angle 2 θ \approx 11.5° and 23° (basal reflections (003) and (006)), and 2 θ \approx 60° (basal reflection (110)). In this case, the sample with the highest crystallinity was used as the reference. The average size of coherent domains, further referred to as crystallite size (L), of the prepared materials was estimated from the X-ray line broadening (the values of the fullwidth at half-maximum) using the Scherrer equation ($L = 0.9\lambda/\beta \cos\theta$), considering different basal reflections: (003) and (110) reflections for the as-prepared and rehydrated HTCs, or (200) and (220) reflections for mixed oxides. The content of Mg²⁺, M³⁺, and Na⁺ in the samples were analyzed by ICP using Agilent 5100 ICP OES.

Nitrogen physisorption was measured at 77 K for calcined catalysts using a static volumetric adsorption system (TriFlex analyzer, Micromeritics, Norcross, GA, USA). The samples were degassed at 473 K (12 h) prior to N₂ adsorption analysis to obtain a clean surface. The adsorption isotherms were fitted using the Brunauer–Emmett–Teller (BET) method for the specific surface area.

All samples were characterized by the FTIR-ATR (Attenuated Total Reflection) technique. An infrared spectrometer IRAffinity-1 (Shimadzu, Kyoto, Japan) with Quest ATR accessory with a diamond crystal (Specac, Fort Washington, PA, USA) was used to record the FTIR spectra. LabSolution IR software (Shimadzu, Kyoto, Japan) was used as an interface between the spectrometer and the control computer. The spectra were recorded in the 4000–400 cm⁻¹ region using the spectral resolution of 2 cm⁻¹.

TGA-MS examination of the as-prepared and rehydrated HTC samples in an N₂ atmosphere was performed using TG-DTA Setsys Evolution (Setaram, Caluire, France)

instrument in the temperature range of 25–700 °C (the molecular ions $m/z = 18$ and 44 were analyzed).

Temperature programmed desorption (TPD) of CO₂ was carried out using a Micromeritics Instrument, AutoChem II 2920. For desorbed CO₂ detection, both a thermal conductivity detector (TCD) and a quadrupole mass spectrometer (MKS Cirrus 2 Analyzer) with a capillary coupling system were used. A catalyst sample (0.06 g) was placed in a quartz U-shaped tube. Prior to adsorption of CO₂, the catalyst was heated under a helium flow (30 mL·min⁻¹) up to 450 °C and kept at 450 °C for 60 min to remove impurities from the sample. In the following step, the sample was cooled down to an adsorption temperature of 40 °C. Measured pulses of CO₂ (pulse volume, 5 mL) were injected into the helium gas and carried through the catalyst sample until adsorption saturation. Then, the sample was purged with helium for 60 min to remove physisorbed CO₂. Afterwards, the linear temperature program (10 °C min⁻¹) was started at a temperature of 40 °C, and the sample was heated up to a temperature of 600 °C. The amount of the desorbed CO₂ was determined by calibration.

The sample morphology was investigated using scanning electron microscopy (SEM) with an FEG electron gun (FIB-SEM TESCAN LYRA3GMU, Brno, Czech Republic) at the acceleration voltage of 10 kV. Prior to the SEM measurement, the sample was placed on a carbon conductive tape and coated by a 5 nm thin gold layer in a sputter coater (Quorum Q150R S, Emitech SC7640 Sputter Coater, Polaron, Laughton, UK).

3.3. Catalytic Tests

Acetone (99.98%, Penta, Czech Republic) and furfural (99%, Sigma-Aldrich) were used as reactants in all catalytic experiments.

It was shown in our recent article [45] that acid impurities in furfural could influence the performance of solids with basic properties in aldol condensation, and that catalyst was partially spent for the neutralization of the acid impurities. Moreover, a routine distillation of an as-received furfural had only a temporary effect on the properties of a furfural source, which was readily re-oxidized and became acidic even if stored in a dark place at decreased temperature. Therefore, it was difficult to maintain the stability and reproducibility of the performance of basic catalysts in aldol condensation. Thus, in the present study, an as-received furfural was first distilled using a vacuum rotator-evaporator and then stabilized by 2,6-di-tert-butyl-4-methylphenol (DBMP, 99%, Sigma-Aldrich) using weight ratio DBMP/Furfural = 0.04). In separate experiments, it was established that the addition DBMP to furfural preserved the properties of furfural as a reagent for aldol condensation for at least 3–4 weeks, which was visually observed by the absence of darkening of this compound during storage. On the other hand, DBMP did not influence the performance of neither mixed oxides nor rehydrated HTCs catalysts in aldol condensation.

Aldol condensation of the stabilized furfural with acetone was carried out in a 100 mL stirred batch reactor (a glass flask reactor) at a temperature of either 50 °C in case of mixed oxides or 25 °C in case of rehydrated HTCs at ambient pressure. The mixture of either 37.9 g of acetone and 6.27 g of furfural (acetone to furfural molar ratio 10:1) or 18.95 g of acetone and 6.27 g of furfural (acetone to furfural molar ratio 5:1) was used for experiments with the mixed oxides or the rehydrated HTCs correspondingly. The catalyst used in the experiments was prepared on the basis of 1 g of an as-prepared hydrotalcite, which corresponded to 0.6 to 0.7 g of calcined catalyst (mixed oxide). Prior to the catalytic tests, the reaction mixture was stirred at 400 rpm and stabilized at reaction temperature. The loss of acetone during the catalytic experiments was prevented by using a cooler-condenser above the reactor. After that, the necessary amount of MgM-C (a mixed oxide powder, freshly calcined in a muffle oven at 450 °C and stored in a desiccator) or MgM-R (a freshly rehydrated HTC, filtered with Buchner funnel) was added, and the reaction was carried out for 180 min at 400 rpm. It was previously established that the reaction was limited neither by external nor internal mass transfer under the chosen reaction conditions (in tests with changing stirring rate and catalyst particle size [34]). Liquid

reaction products were periodically withdrawn from the reactor during the experiment, centrifugated, filtered, diluted with methanol (1:25 by volume), and analyzed by Agilent 7820 GC unit equipped with a flame ionization detector (FID), using a HP-5 capillary column (30 m/0.32 mm ID/0.25 μm). Catalytic results on aldol condensation of furfural and acetone were described by conversion and selectivity parameters that were calculated as follows [34,41]:

Reactant conversion (t) (mol%) = $100 \times (\text{reactant}_{t=0} - \text{reactant}_{t=t}) / \text{reactant}_{t=0}$, where t stands for reaction time

Selectivity to product i = $100 \times (\text{mole of reactant converted to product i}) / (\text{total moles of reactant converted})$

Carbon balance was monitored in all experiments as the total number of carbon atoms detected in each organic compound with C_n atoms (where $n = 3, 5, 8, \dots$, etc.) divided by the initial number of carbon atoms in the F + Ac feed:

C balance (%) = $(3 \text{ mol C}_3 + 5 \text{ mol C}_5 \dots + n \text{ mol C}_n) / (3 \text{ mol C}_3(t=0) + 5 \text{ mol C}_5(t=0))$.

Each catalytic experiment was repeated several (at least 3) times to prove the reproducibility of the obtained results (with experimental error evaluated as $\pm 5\%$).

4. Conclusions

To elucidate the impact of the nature of M^{3+} cation in MgM^{3+} hydrotalcites (HTCs) on the physico-chemical properties and the catalytic performance of the corresponding mixed oxides and rehydrated HTCs, four samples of MgM^{3+} HTCs ($\text{M} = \text{Al, Ga, Fe, In}$) were prepared by a precipitation method using the same synthesis protocol. XRD data evidenced that the as-prepared materials were phase-pure HTCs, nevertheless with varied crystallinity. The characterization of the as-prepared samples indicated that the observed difference in the crystallinity could be explained by the difference in their crystallite size, defectiveness, and intergrowth of the layered structure, rather than by the presence of an amorphous phase. The CO_2 -TPD study showed that the concentration of the basic sites in MgM^{3+} mixed oxides differed, and it gradually decreased with the growth in the atomic weight of the M^{3+} element. Nevertheless, all mixed oxides had almost the same distribution of the basic site strengths. Interestingly, when the total amount of adsorbed CO_2 was expressed per MgO site, it was the same within the experimental error for all studied mixed oxides. Accordingly, the catalytic performance of the mixed oxides in aldol condensation of furfural and acetone was determined by their basic characteristics. The used 20 min rehydration of the mixed oxides resulted in almost complete (>90%) recovery of the HTC structure with crystallinity values close to those for the as-prepared HTCs. To the best of our knowledge, the successful formation of rehydrated MgIn HTC using pure water at ambient temperature was reported here for the first time. The SEM study evidenced that the rehydration of the mixed oxides resulted in the formation of crystals with irregular and defective lamellar structure, which could explain the slightly decreased crystallinity and the decreased crystallite size of the rehydrated HTCs. The activity of all rehydrated MgM^{3+} HTCs in aldol condensation of furfural and acetone was much higher compared to that of the mixed oxides. Moreover, the difference in furfural conversion observed between the four rehydrated HTCs was obvious, but the observed trend in the activity of the catalysts correlated neither with their crystallinity nor with the atomic weight of the M cation nor with the concentration of the basic sites in the mixed oxides used as precursors. This pointed to the existence of additional factors, for example, the influence of the rehydration conditions that could determine the amount of accessible active sites in these materials and, as a consequence, their catalytic performance. A series of three consecutive experiments with the same catalyst loading demonstrated that the activity of the rehydrated MgM^{3+} catalysts in aldol condensation was fully restored after their separation from the reaction mixture, followed by re-calcination and re-hydration steps. The performed experiments suggest that the rehydrated MgM^{3+} materials ($\text{M} = \text{Al, Ga, Fe, In}$) possess comparable catalytic performance in aldol condensation of furfural and acetone

in terms of activity, selectivity, and stability, being apparently determined by the properties of the “host” component, i.e., magnesium oxide.

Supplementary Materials: The following are available online at <https://www.mdpi.com/article/10.3390/catal11080992/s1>.

Author Contributions: Conceptualization, D.K. and O.K.; methodology, O.K.; investigation, V.K., M.V., D.V., I.P. and V.F.; data curation, V.K.; writing—original draft preparation, V.K. and O.K.; writing—review and editing, D.K. and L.Č.; visualization, V.K.; supervision, O.K.; project administration, D.K.; funding acquisition, O.K. and L.Č. All authors have read and agreed to the published version of the manuscript.

Funding: This research was funded by the Czech Science Foundation, grant number 19-22978S.

Data Availability Statement: Not applicable.

Acknowledgments: The authors are grateful to the Czech Science Foundation for the financial support (Project No. 19-22978S).

Conflicts of Interest: The authors declare no conflict of interest.

References

1. Debecker, D.P.; Gaigneaux, E.M.; Busca, G. Exploring, Tuning, and Exploiting the Basicity of Hydrotalcites for Applications in Heterogeneous Catalysis. *Chem. Eur. J.* **2009**, *15*, 3920–3935. [CrossRef]
2. Abelló, S.; Medina, F.; Tichit, D.; Pérez-Ramírez, J.; Groen, J.C.; Sueiras, J.E.; Salagre, P.; Cesteros, Y. Aldol Condensations Over Reconstructed Mg–Al Hydrotalcites: Structure–Activity Relationships Related to the Rehydration Method. *Chem. Eur. J.* **2005**, *11*, 728–739. [CrossRef] [PubMed]
3. Tichit, D.; Coq, B. Catalysis by Hydrotalcites and Related Materials. *Cattech* **2003**, *7*, 206–217. [CrossRef]
4. Tichit, D.; Bennani, M.N.; Figueras, F.; Tessier, R.; Kervennal, J. Aldol condensation of acetone over layered double hydroxides of the meixnerite type. *Appl. Clay Sci.* **1998**, *13*, 401–415. [CrossRef]
5. Climent, M.J.; Corma, A.; Fornés, V.; Guil-Lopez, R.; Iborra, S. Aldol Condensations on Solid Catalysts: A Cooperative Effect between Weak Acid and Base Sites. *Adv. Synth. Catal.* **2002**, *344*, 1090–1096. [CrossRef]
6. Guida, A.; Lhouty, M.H.; Tichit, D.; Figueras, F.; Geneste, P. Hydrotalcites as base catalysts. Kinetics of Claisen–Schmidt condensation, intramolecular condensation of acetylacetone and synthesis of chalcone. *Appl. Catal. A-Gen.* **1997**, *164*, 251–264. [CrossRef]
7. Kikhtyanin, O.; Hora, L.; Kubička, D. Unprecedented selectivities in aldol condensation over Mg–Al hydrotalcite in a fixed bed reactor setup. *Catal. Commun.* **2015**, *58*, 89–92. [CrossRef]
8. Červený, J.; Šplíchalová, J.; Kačer, P.; Kovanda, F.; Kuzma, M.; Červený, L. Molecular shape selectivity of hydrotalcite in mixed aldol condensations of aldehydes and ketones. *J. Mol. Catal. A Chem.* **2008**, *285*, 150–154. [CrossRef]
9. Othman, M.R.; Helwani, Z.; Martunus; Fernando, W.J.N. Synthetic hydrotalcites from different routes and their application as catalysts and gas adsorbents: A review. *Appl. Organomet. Chem.* **2009**, *23*, 335–346. [CrossRef]
10. Sideris, P.J.; Nielsen, U.G.; Gan, Z.; Grey, C.P. Mg/Al ordering in layered double hydroxides revealed by multinuclear NMR spectroscopy. *Science* **2008**, *321*, 113–117. [CrossRef]
11. Nishimura, S.; Takagaki, A.; Ebitani, K. Characterization, synthesis and catalysis of hydrotalcite-related materials for highly efficient materials transformations. *Green Chem.* **2013**, *15*, 2026–2042. [CrossRef]
12. Sels, B.F.; de Vos, D.E.; Jacobs, P.A. Hydrotalcite-like anionic clays in catalytic organic reactions. *Catal. Rev. Sci. Eng.* **2011**, *43*, 443–488. [CrossRef]
13. Cavani, F.; Trifiro, F.; Vaccari, A. Hydrotalcite-type anionic clays: Preparation, properties and applications. *Catal. Today* **1991**, *11*, 173–301. [CrossRef]
14. Debek, R.; Motak, M.; Grzybek, T.; Galvez, M.E.; da Costa, P. A Short Review on the Catalytic Activity of Hydrotalcite-Derived Materials for Dry Reforming of Methane. *Catalysts* **2017**, *7*, 32. [CrossRef]
15. Takehira, K.; Shishido, T. Preparation of supported metal catalysts starting from hydrotalcites as the precursors and their improvements by adopting “memory effect”. *Catal. Surv. Asia* **2007**, *11*, 1–30. [CrossRef]
16. Kikhtyanin, O.; Capek, L.; Tisler, Z.; Velvarská, R.; Panasewicz, A.; Diblíková, P.; Kubíčka, D. Physico-Chemical Properties of MgGa Mixed Oxides and Reconstructed Layered Double Hydroxides and Their Performance in Aldol Condensation of Furfural and Acetone. *Front. Chem.* **2018**, *6*, 176. [CrossRef] [PubMed]
17. Kocík, J.; Frolich, K.; Perková, I.; Horáček, J. Pyroaurite-based Mg–Fe mixed oxides and their activity in aldol condensation of furfural with acetone: Effect of oxide composition. *J. Chem. Technol. Biotechnol.* **2019**, *94*, 435–445. [CrossRef]
18. Tichit, D.; Lutić, D.; Coq, B.; Durand, R.; Teissier, R. The aldol condensation of acetaldehyde and heptanal on hydrotalcite-type catalysts. *J. Catal.* **2003**, *219*, 167–175. [CrossRef]

19. Smolakova, L.; Frolich, K.; Kocik, J.; Kikhtyanin, O.; Capek, L. Surface Properties of Hydrotalcite-Based Zn(Mg)Al Oxides and Their Catalytic Activity in Aldol Condensation of Furfural with Acetone. *Ind. Eng. Chem. Res.* **2017**, *56*, 4638–4648. [[CrossRef](#)]
20. Sánchez-Cantú, M.; Pérez-Díaz, L.M.; Rubio-Rosas, E.; Abril-Sandoval, V.H.; Merino-Aguirre, J.G.; Reyes-Cruz, F.M.; Orea, L. MgZnAl hydrotalcite-like compounds preparation by a green method: Effect of zinc content. *Chem. Pap.* **2014**, *68*, 638–649. [[CrossRef](#)]
21. Hernández, W.Y.; Aliç, F.; Verberckmoes, A.; van der Voort, P. Tuning the acidic–basic properties by Zn-substitution in Mg–Al hydrotalcites as optimal catalysts for the aldol condensation reaction. *J. Mater. Sci.* **2017**, *52*, 628–642. [[CrossRef](#)]
22. Reichle, W.T. Catalytic reactions by thermally activated, synthetic, anionic clay minerals. *J. Catal.* **1985**, *94*, 547–557. [[CrossRef](#)]
23. Fakhfakh, N.; Cognet, P.; Cabassud, M.; Lucchese, Y.; de los Ríos, M.D. Stoichio-Kinetic Modeling and Optimization of Chemical Synthesis: Application to the Aldolic Condensation of Furfural on Acetone. *Chem. Eng. Process.* **2008**, *47*, 349–362. [[CrossRef](#)]
24. Climent, M.J.; Corma, A.; Garcia, H.; Guil-Lopez, R.; Iborra, S.; Fornes, V. Acid-base bifunctional catalysts for the preparation of fine chemicals: Synthesis of jasminaldehyde. *J. Catal.* **2001**, *197*, 385–393. [[CrossRef](#)]
25. Li, X.; Sun, J.; Shao, S.; Hu, X.; Cai, Y. Aldol condensation/hydrogenation for jet fuel from biomass-derived ketone platform compound in one pot. *Fuel Process. Technol.* **2021**, *215*, 106768. [[CrossRef](#)]
26. Han, F.; Xu, J.; Li, G.; Xu, J.; Wang, A.; Cong, Y.; Zhang, T.; Li, N. Synthesis of renewable aviation fuel additives with aromatic aldehydes and methyl isobutyl ketone under solvent-free conditions. *Sustain. Energy Fuels* **2021**, *5*, 556–563. [[CrossRef](#)]
27. Sacia, E.R.; Balakrishnan, M.; Deaner, M.H.; Goulas, K.A.; Toste, F.D.; Bell, A.T. Highly Selective Condensation of Biomass-Derived Methyl Ketones as a Source of Aviation Fuel. *ChemSusChem* **2015**, *8*, 1726–1736. [[CrossRef](#)] [[PubMed](#)]
28. Kikhtyanin, O.; Kadlec, D.; Velvarská, R.; Kubička, D. Using Mg-Al Mixed Oxide and Reconstructed Hydrotalcite as Basic Catalysts for Aldol Condensation of Furfural and Cyclohexanone. *ChemCatChem* **2018**, *10*, 1464–1475. [[CrossRef](#)]
29. Stadler, B.M.; Wulf, C.; Werner, T.; Tin, S.; de Vries, J.G. Catalytic Approaches to Monomers for Polymers Based on Renewables. *ACS Catal.* **2019**, *9*, 8012–8067. [[CrossRef](#)]
30. Chang, H.; Gilcher, E.B.; Huber, G.W.; Dumesic, J.A. Synthesis of performance-advantaged polyurethanes and polyesters from biomass-derived monomers by aldol-condensation of 5-hydroxymethyl furfural and hydrogenation. *Green Chem.* **2021**. [[CrossRef](#)]
31. Thomas, G.S.; Kamath, P.V. Reversible thermal behavior of the layered double hydroxides (LDHs) of Mg with Ga and In. *Mater. Res. Bull.* **2005**, *40*, 671–681. [[CrossRef](#)]
32. Aramendía, M.A.; Avilés, Y.; Benítez, J.A.; Borau, V.; Jiménez, C.; Marinas, J.M. Comparative study of Mg/Al and Mg/Ga layered double hydroxides. *Microporous Mesoporous Mater.* **1999**, *29*, 319–328. [[CrossRef](#)]
33. Li, F.; Jiang, X.; Evans, D.G.; Duan, X. Structure and Basicity of Mesoporous Materials from Mg/Al/In Layered Double Hydroxides Prepared by Separate Nucleation and Aging Steps Method. *J. Porous Mater.* **2005**, *12*, 55–63. [[CrossRef](#)]
34. Kikhtyanin, O.; Tišler, Z.; Velvarská, R.; Kubička, D. Reconstructed Mg-Al hydrotalcites prepared by using different rehydration and drying time: Physico-chemical properties and catalytic performance in aldol condensation. *Appl. Catal. A Gen.* **2017**, *536*, 85–96. [[CrossRef](#)]
35. Climent, M.J.; Corma, A.; Iborra, S.; Velty, A. Synthesis of methylpseudoionones by activated hydrotalcites as solid base catalysts. *Green Chem.* **2002**, *4*, 474–480. [[CrossRef](#)]
36. Roelofs, J.C.A.A.; Lensveld, D.J.; van Dillen, A.J.; de Jong, K.P. On the Structure of Activated Hydrotalcites as Solid Base Catalysts for Liquid-Phase Aldol Condensation. *J. Catal.* **2001**, *203*, 184–191. [[CrossRef](#)]
37. Figueras, F.; Lopez, J.; Sanchez-Valente, J.; Vu, T.T.H.; Clacens, J.-M.; Palomeque, J. Isophorone Isomerization as Model Reaction for the Characterization of Solid Bases: Application to the Determination of the Number of Sites. *J. Catal.* **2002**, *211*, 144–149. [[CrossRef](#)]
38. Pérez-Ramírez, J.; Abello, S.; van der Pers, N.M. Memory Effect of Activated Mg–Al Hydrotalcite: In Situ XRD Studies during Decomposition and Gas-Phase Reconstruction. *Chem. Eur. J.* **2007**, *13*, 870–878. [[CrossRef](#)] [[PubMed](#)]
39. Sharma, S.K.; Parikh, P.A.; Jasra, R.V. Reconstructed Mg/Al hydrotalcite as a solid base catalyst for synthesis of jasminaldehyde. *Appl. Catal. A Gen.* **2010**, *386*, 34–42. [[CrossRef](#)]
40. Hibino, T.; Tsunashima, A. Calcination and rehydration behavior of Mg-Fe-CO₃ hydrotalcite-like compounds. *J. Mater. Sci. Lett.* **2000**, *19*, 1403–1405. [[CrossRef](#)]
41. Kikhtyanin, O.; Čapek, L.; Smoláková, L.; Tišler, Z.; Kadlec, D.; Lhotka, M.; Diblíková, P.; Kubička, D. Influence of Mg–Al Mixed Oxide Compositions on Their Properties and Performance in Aldol Condensation. *Ind. Eng. Chem. Res.* **2017**, *56*, 13411–13422. [[CrossRef](#)]
42. Kikhtyanin, O.; Lesnik, E.; Kubička, D. The occurrence of Cannizzaro reaction over Mg-Al hydrotalcites. *Appl. Catal. A Gen.* **2016**, *525*, 215–225. [[CrossRef](#)]
43. Xu, C.; Gao, Y.; Liu, X.; Xin, R.; Wang, Z. Hydrotalcite reconstructed by in situ rehydration as a highly active solid base catalyst and its application in aldol condensations. *RSC Adv.* **2013**, *3*, 793–801. [[CrossRef](#)]
44. Abelló, S.; Vijaya-Shankar, D.; Pérez-Ramírez, J. Stability, reutilization, and scalability of activated hydrotalcites in aldol condensation. *Appl. Catal. A Gen.* **2008**, *342*, 119–125. [[CrossRef](#)]
45. Kikhtyanin, O.; Korolova, V.; Spencer, A.; Dubnová, L.; Shumeiko, B.; Kubička, D. On the influence of acidic admixtures in furfural on the performance of MgAl mixed oxide catalysts in aldol condensation of furfural and acetone. *Catal. Today* **2021**, *367*, 248–257. [[CrossRef](#)]